Swinburne Research Bank
http://researchbank.swinburne.edu.au

Author: Nazari, Ali; Sanjayan, Jay G.
Title: Modelling of fracture strength of functionally graded geopolymer
Year: 2014
Journal: Construction and Building Materials
Volume: 58
Pages: 38-45
URL: http://doi.org/10.1016/j.conbuildmat.2014.01.096

Copyright: Copyright © 2014 Published by Elsevier B.V. All rights reserved. This is the author's version of a work that was accepted for publication in Construction and Building Materials. Changes resulting from the publishing process, such as peer review, editing, corrections, structural formatting, and other quality control mechanisms may not be reflected in this document. Changes may have been made to this work since it was submitted for publication. A definitive version was subsequently published in Construction and Building Materials, [VOL 58, 2014] DOI: 10.1016/j.conbuildmat.2014.01.096

This is the author's version of the work, posted here with the permission of the publisher for your personal use. No further distribution is permitted. You may also be able to access the published version from your library.

The definitive version is available at: http://doi.org/10.1016/j.conbuildmat.2014.01.096

Modelling of fracture strength of functionally graded geopolymer

Ali Nazari* and Jay G. Sanjayan

Centre for Sustainable Infrastructure, Faculty of Science, Engineering and Technology, Swinburne University of Technology, Victoria, 3122, Australia

* Corresponding author, Tel: +61 3 92148370, Email: alinazari@swin.edu.au

ABSTRACT

In the current paper, fracture strength of a functionally graded geopolymer was analytically modelled for crack propagation in two possible perpendicular situations with respect to the functionally graded region. Functionally graded geopolymer was produced by pouring and subsequent vibration of two layers of different alkali activated fly ash-based geopolymers into the moulds. The thickness of functionally graded region was determined equal to 18.6 mm through evaluating Si/Al ratio obtained from EDS. In modelling procedure of both crack configurations, the functionally graded region was considered to have 372 layers with the thickness of 50 μm and the fracture strength of the geopolymeric specimen in functionally graded region was related to the fracture strength of the constituent layers. To represent the variation of surface energy and elastic modulus in functionally graded region, three different functions including exponential, power-law and linear were considered. The obtained results from the proposed model show a good agreement with that of obtained through experimental procedure.

Keywords: functionally graded geopolymeric region; analytical modelling; fracture strength; crack growth energy

1. Introduction

The demands on acquiring reliable cementitious mixture for different operational conditions as well as the desire to their production with lower costs enforce scientists to survey into new concepts in concrete specimens. One possible method to improve the properties of concrete specimens in an affordable way is to produce "functionally graded concrete" (FGC) which for the first time was presented in 2006 [1].

In FGMs as multi-phase systems, to obtain unique mechanical, thermal and electrical properties, the composition changes gradually in some directions. They are distinguished in this way from the conventional composites that have discrete and piecewise nature as well as sharp interfaces [2]. The main advantage of gradual change in the graded region is reduction of stress concentration. Additionally, by arranging the appropriate constituent materials, one may access the required property that unattainable not only by a homogenous material, but by a complicated laminate composite. Finally, delamination which is caused during crack propagation into composite structure does not occur in FGMs [2, 3]. Although delamination may increase the fracture energy of the composite materials with respect to FGMs, this behaviour is avoided in concrete structures where homogeneity and continuity of a specific cementitious section are of the main importance.

Wen et al. [1] examined two kinds of single-layer concrete specimens and functionally gradient structure concrete with three different Surface-layer thicknesses against rapid chloride attack and accelerated steel bar corrosion tests. They found that FGC system is able to improve resistance to chloride attack and hence reduce the corrosion of the incorporated steel bars. Dias et al [4] statistically analysed different designs to choose formulations and present ideas for the production of functionally graded PVA fibre cement components. Through grading PVA fibres, they obtained affordable concrete with reduced total fibre volume without a significant decrease on modulus of rupture of FGC. Shen et al.

[5] examined flexural strength of four-layer functionally graded fibre-reinforced cement concrete by changing the content of PVA fibres in the layers. Fibre volume fraction was linearly changed from 0 % in the compression zone to 2 % in the tensile zone. The results show 50 % improvement in flexural strength as well as comparable fracture energy with respect to homogeneous PVA fibre-reinforced concrete with same volume fraction of PVA fibres. Quek et al. [6] developed functionally graded polyethylene fibre-reinforced concrete specimens for resisting to high velocity impact tests. The results showed that FGC specimens have superior impact energy with respect to the normal concrete. This short review indicates the abilities of functionally graded concrete systems to improve the required properties affordably. Hence, functionally graded geopolymer (FGG) specimens may act in a similar way as well.

Geopolymers (alkali activated binders), eco-friendly materials with much lower CO_2 emissions produced from different sources such as fly ash [7-9], slags [10-12] and metakaolin [13], individually or together, are considered as the main possible substitution materials of ordinary Portland cement- (OPC)-based concrete. The most attractive constructional raw material for geopolymer production is fly ash because of its availability and cheaper price. Fly ash-based geopolymers are made from mixtures of fly ash as aluminosilicate source and a regular silica-rich alkali activator which normally is a combination of sodium silicate or potassium silicate together with sodium hydroxide or potassium hydroxide [7-9]. In the current study, FGG structures are introduced to attain unique mechanical properties that could not be obtained by a single homogenous geopolymer or even geopolymer composite. Development of FGG structures in the future will deliver reasonable compressive, flexural and splitting tensile strength with the other demanded properties that are not wholly achieved in a homogeneous cementitious material.

The aim of the present study is to model fracture strength of the proposed fly ash

based FGG structure for cracks perpendicular to the functionally graded region. Two individual models were presented that in both of them, the fracture strength of the specimen was considered as the sum of the fracture strength of homogeneous layers together with the constituent layers of functionally graded region.

2. Experimental procedure

Two fine fly ashes with the particle size distributions obtained by ASTM C115 [14] standard illustrated in Fig. 1 and chemical compositions given in Table 1 were considered for this study. The average particle size of fly ash type I and type II were 14 and 9 μm respectively. Alkali activation was done by a mixture of sodium hydroxide (NaOH) and sodium silicate. The concentration of NaOH was 14 M and sodium silicate was used as-received. High NaOH concentration causes higher strengths due to more convenient dissolution of Si^{4+} and Al^{3+} from fly ash to alkali activator [15], and hence to reduce the possibility of weakening the aluminosilicate structure as well as reducing the scattered data. The chemical composition of sodium silicate has been given in Table 1. Sodium silicate to NaOH weight ratio in alkali activator was considered 2.5 for both geopolymeric mixtures since this ratio is used in a considerable number of geopolymer-related works reported in the literature [16].

Two geopolymeric pastes were prepared. The first (G1) was made by mixing 3:1 fly ash type I and alkali activator weight ratio. The second geopolymer (G2) was made in same procedure but by using fly ash type II.

To make FGG structure, geopolymers mixtures were poured in two layers. The mould was half-filled by G1 mixture and vibrated for 45 s to avoid air bubbles. After that, G2 was poured as the top layer and again vibrated for 45 s to avoid air bubbles as well as to provide

diffusion of G1 and G2 mixtures into each other. The vibration was carried out on a vibration table by the frequency of 15 Hz. The reason for using a low frequency was due to reducing the possibility of mixing the whole pastes into each other. In pre-curing stage, the moulds were left for 24 h while covered with a polyester sheet. After 24 h, the specimens were de-moulded and were oven cured for 24 h at 70 ^{o}C and finally were cured for additional 27 days in room temperature. The method of production FGG structure has been illustrated schematically in Fig. 2.

To determine the boundary conditions required for modelling process, monolithic geopolymeric specimens were made from G1 and G2 mixtures. Both mixtures were made in the same manner mentioned for FGG structure where the two poured layers were similar.

To determine modulus of elasticity of the monolithic specimens, cylindrical samples with the diameter of 150 mm and the length of 300 mm were prepared and tested in accordance to the ASTM C469-87 [17].

Fracture strength of the FGG structure as well as monolithic specimens was acquired by a single-notched edge beam under three-point loading with the dimensions of 10 cm × 10 cm × 65 cm. The span to depth ratio was four and the width of crack was considered 5 mm with a crack tip radius of 1 mm. The width and radius of crack were selected in such way that have the minimum impact on abrupt crack propagation, and assure that the crack propagates from the demanded point.

Fig. 3 shows schematically the configuration of the cracks with respect to the functionally graded region. In the first configuration (which is called CP1 here) the crack is perpendicular to the graded region and incorporates the whole layers of this region. The crack propagates along the graded region. In the second configuration (which is called CP2 here) the crack is perpendicular to the graded region while propagates across the layers of the

graded region. The similar structures to CP1 and CP2 in laminated composites with sharp interfaces are called crack divider and crack arrester configuration and may be considered as an indicative definition. However, dividing or arresting cracks are occurred during delamination of the layered composites and do not reflect the correct connotation here. These can only show the morphology of cracks with respect to the layers of functionally graded regions.

To determine the depth of functionally graded region, SEM equipped with EDS facility was used. However, additional analysing methods such as XRD, FT-IT, etc. may be beneficial to further examinations of the quality and microstructure of homogeneous and functionally graded regions [18, 19]. At first, the mean Si/Al ratio for monolithic G1 and G2 specimens was determined. This was done by considering 2 different samples of each mixture and five analyses per sample. In other words, for each sample, the average Si/Al height of EDS peak ratio for each monolithic specimen was achieved by testing 10 points of the specimen. The points were randomly selected to represent a more reliable value instead of using the data of a single point. Additionally, the results which were too far from the average value were neglected in the calculations. After that, to determine the boundary between functionally graded region and G1 mixture, in SEM micrograph of the FGG structure, by the aim of suitable software, several lines parallel to the imaginary graded region were drawn. The distance between the parallel lines was 50 micron. The chemical composition of these line was achieved from 10 points and the average Si/Al ratio was achieved. The boundary was considered approximately in the middle distance of two parallel lines where the first line had the same height of EDS peak Al/Si ratio to G1 mixture and the second had height of EDS peak Si/Al ratio with a gradual change of 5 %. Same procedure was carried out for the boundary between functionally graded region and G2 mixture.

3. Results, discussion and modelling

Fig. 4 shows the fracture surface of G1 and G2 monolithic specimens. Both microstructures show a brittle fracture and are suitable for the modelling procedure which has been carried out in the current study. For functionally graded region of the specimen with FGG structure (Fig. 4c), a mixture of both fracture surface may show the gradual change of properties in this region. The depth of functionally graded region was estimated to be about 18.6 mm through the method described above.

Furthermore, fracture strength, modulus of elasticity and surface energy (which is calculated by Griffith theory [20]) of G1 and G2 specimens have been shown in Table 2. Fracture strength of the both FGG specimens with crack configurations of CP1 and CP2 has been given in Tables 3-5. It is obvious that the fracture strength of the both FGG structures is a value between those of G1 and G2 specimens. Hence, the fracture strength of the FGG structure depends on the degree of contribution of each region.

FGG sample can be considered as a specimen with three separate region inclusive G1, G2 an FGG zones. For a brittle homogeneous specimen with width *w*, an initial crack length of a_0, modulus elasticity of *E* and surface energy of γ, fracture strength in accordance to the Griffith law [20] can be stated as Eq. (1):

$$\sigma_f = \sqrt{\frac{2E.\gamma}{\pi.a_0}}.\sqrt{sec\left(\frac{\pi.a_0}{w}\right)} \quad (1)$$

Fracture strength of G1 and G2 specimens has been given in Table 2 and hence, γ of both mixtures was calculated and has been given in Table 2 as well. For FGG structure, calculation of fracture parameters is not straightforward. One may consider the graded region as a structure consisting of *m* parallel layers perpendicular to the load direction in this study. The characteristics of these constituent layers are different and their variation in the graded

region may obey a regular or irregular pattern. For the aim of modelling in the current study, the thickness of each layer in the FGG region was considered 50 micron. Selection of a function to state these variations significantly affect the results of modelling procedure. The most common functions used in the literature to represent the variation of properties across the graded region are linear [21], power-law [22] and exponential [23] functions. In the present work, these three types of functions were used to state the variations of elastic modulus and surface energy in the functionally graded regions:

$$E_i = A.exp(BX_i) \tag{2}$$

$$E_i = A.B^{X_i} \tag{3}$$

$$E_i = A.X_i + B \tag{4}$$

$$\gamma_i = C.exp(D.X_i) \tag{5}$$

$$\gamma_i = C.D^{X_i} \tag{6}$$

$$\gamma_i = C.X_i + D \tag{7}$$

where *A*, *B*, *C* and *D* are constants and should be determined by considering boundary conditions. The two boundary conditions for calculating the variations of *E* in the graded region are:

If $X = X_{G1}$ Then $E = E_{G1}$, and

If $X = X_{G2}$ Then $E = E_{G2}$,

where X_{G1} and X_{G2} are the position of G1 and G2 regions respectively and E_{G1} and E_{G2} are modulus of elasticity of G1 and G2 regions respectively.

By substituting the boundary conditions into Eqs. (2)-(4) and further simplification, the Eqs. (8)-(10) will be obtained for exponential, power-law and linear functions

respectively to state variations of E across the functionally graded region:

$$E_i = E_{G1}.\left(\frac{E_{G1}}{E_{G2}}\right)^{\left(\frac{X_i - X_{G1}}{X_{G1} - X_{G2}}\right)} \tag{8}$$

$$E_i = E_{G1}.\left(\frac{X_i}{X_{G1}}\right)^{\left[ln\left(\frac{E_{G2}}{E_{G1}}\right)/ln\left(\frac{X_{G2}}{X_{G1}}\right)\right]} \tag{9}$$

$$E_i = \frac{E_{G1}(X_i - X_{G2}) - E_{G2}(X_i - X_{G1})}{X_{G1} - X_{G2}} \tag{10}$$

For variations of γ across the functionally graded region, similar procedure is carried out and the following boundary conditions are considered:

If $X = X_{G1}$ Then $\gamma = \gamma_{G1}$, and

If $X = X_{G2}$ Then $\gamma = \gamma_{G2}$,

where γ_{G1} and γ_{G2} are modulus of elasticity of G1 and G2 regions respectively.

Hence, Eqs. (11)-(14) are obtained to state the variations of γ across the functionally graded region by exponential, power-law and linear functions respectively:

$$\gamma_i = \gamma_{G1}.\left(\frac{\gamma_{G1}}{\gamma_{G2}}\right)^{\left(\frac{X_i - X_{G1}}{X_{G1} - X_{G2}}\right)} \tag{12}$$

$$\gamma_i = \gamma_{G1}.\left(\frac{X_i}{X_1}\right)^{\left[ln\left(\frac{\gamma_{G2}}{\gamma_{G1}}\right)/ln\left(\frac{X_{G2}}{X_{G1}}\right)\right]} \tag{13}$$

$$\gamma_i = \frac{\gamma_{G1}(X_i - X_{G2}) - \gamma_{G2}(X_i - X_{G1})}{X_{G1} - X_{G2}} \tag{14}$$

3.1. Modelling of fracture strength of CP1 crack configuration

In CP1 condition, the whole homogeneous G1 and G2 regions as well as functionally graded region are incorporated by the crack. It can be assumed that each layer in functionally graded region contribute in determining the final strength in accordance to the rule of

mixtures. In other words, the share of each layer is its corresponding fracture strength, $\sigma^{i}_{f,CP1}$, multiplied with its volume fraction, f_i, as following:

$$\sigma^{i}_{f,CP1} = \sqrt{\frac{2E_i.\gamma_i}{\pi.a_0}}.\sqrt{sec\left(\frac{\pi.a_0}{w}\right)} \times f_i \tag{15}$$

Therefore, the fracture strength of the composite structure containing G1 and G1 monolithic regions together with functionally graded region could be given by Eq. (16):

$$\sigma_{f,CP1} = \sum_{i=1}^{m} \sqrt{\frac{2E_i.\gamma_i}{\pi.a_0}}.\sqrt{sec\left(\frac{\pi.a_0}{w}\right)} \times f_i + \sigma_{f,G1} \times f_{G1} + \sigma_{f,G2} \times f_{G2} \tag{16}$$

where $\sigma_{f,G1}$ and $\sigma_{f,G2}$ are fracture strength of G1 and G2 regions respectively and f_{G1} and f_{G2} are volume fractions of G1 and G2 regions respectively.

Finally, the model is completed by substituting E_i and γ_i with their corresponding function. According to the equations given for E_i and γ_i in the present work, nine possible models are derived as following:

For exponential variation of both E_i and γ_i in the graded region:

$$\sigma^{1}_{f,CP1} = \sum_{i=1}^{m} \sqrt{\frac{2E_{G1}.\gamma_{G1}.\left(\frac{E_{G1}.\gamma_{G1}}{E_{G2}.\gamma_{G2}}\right)^{\left(\frac{X_i - X_{G1}}{X_{G1} - X_{G2}}\right)}}{\pi.a_0}}.\sqrt{sec\left(\frac{\pi.a_0}{w}\right)} \times f_i + \sigma_{f,G1} \times f_{G1} + \sigma_{f,G2} \times f_{G2} \tag{17}$$

For exponential variation of E_i and power-law variation of γ_i in the graded region:

$$\sigma^{2}_{f,CP1} = \sum_{i=1}^{m} \sqrt{\frac{2E_{G1}.\gamma_{G1}.\left(\frac{E_{G1}}{E_{G2}}\right)^{\left(\frac{X_i - X_{G1}}{X_{G1} - X_{G2}}\right)}.\left(\frac{X_i}{X_{G1}}\right)^{\left[ln\left(\frac{\gamma_{G2}}{\gamma_{G1}}\right)/ln\left(\frac{X_{G2}}{X_{G1}}\right)\right]}}{\pi.a_0}}.\sqrt{sec\left(\frac{\pi.a_0}{w}\right)} \times f_i + \sigma_{f,G1} \times f_{G1} + \sigma_{f,G2} \times f_{G2} \tag{18}$$

For exponential variation of E_i and linear variation of γ_i in the graded region:

$$\sigma_{f,CP1}^{3} = \sum_{i=1}^{m} \sqrt{\frac{2E_{G1}.\left(\frac{E_{G1}}{E_{G2}}\right)^{\left(\frac{X_i - X_{G1}}{X_{G1} - X_{G2}}\right)}.\left(\frac{\gamma_{G1}(X_i - X_{G2}) - \gamma_{G2}(X_i - X_{G1})}{X_{G1} - X_{G2}}\right)}{\pi.a_0}}.\sqrt{sec\left(\frac{\pi.a_0}{w}\right)} \times f_i + \sigma_{f,G1} \times f_{G1} +$$

$$\sigma_{f,G2} \times f_{G2} \quad (19)$$

For power-law variation of E_i and exponential variation of γ_i in the graded region:

$$\sigma_{f,CP1}^{4} = \sum_{i=1}^{m} \sqrt{\frac{2E_{G1}.\gamma_{G1}.\left(\frac{X_i}{X_1}\right)^{\left[ln\left(\frac{E_{G2}}{E_{G1}}\right)/ln\left(\frac{X_{G2}}{X_{G1}}\right)\right]}.\left(\frac{\gamma_{G1}}{\gamma_{G2}}\right)^{\left(\frac{X_i - X_{G1}}{X_{G1} - X_{G2}}\right)}}{\pi.a_0}}.\sqrt{sec\left(\frac{\pi.a_0}{w}\right)} \times f_i + \sigma_{f,G1} \times f_{G1} +$$

$$\sigma_{f,G2} \times f_{G2} \quad (20)$$

For power-law variation of both E_i and γ_i in the graded region:

$$\sigma_{f,CP1}^{5} = \sum_{i=1}^{m} \sqrt{\frac{2E_{G1}.\gamma_{G1}.\left(\frac{X_i}{X_{G1}}\right)^{\left[ln\left(\frac{E_{G2}}{E_{G1}}\right).ln\left(\frac{\gamma_{G2}}{\gamma_{G1}}\right)/\left[ln\left(\frac{X_{G2}}{X_{G1}}\right)\right]^2\right]}}{\pi.a_0}}.\sqrt{sec\left(\frac{\pi.a_0}{w}\right)} \times f_i + \sigma_{f,G1} \times f_{G1} + \sigma_{f,G2} \times$$

$$f_{G2} \quad (21)$$

For power-law variation of E_i and linear variation of γ_i in the graded region:

$$\sigma_{f,CP1}^{6} = \sum_{i=1}^{m} \sqrt{\frac{2E_{G1}.\left(\frac{X_i}{X_{G1}}\right)^{\left[ln\left(\frac{E_{G2}}{E_{G1}}\right)/ln\left(\frac{X_{G2}}{X_{G1}}\right)\right]}.\left(\frac{\gamma_{G1}(X_i - X_{G2}) - \gamma_{G2}(X_i - X_{G1})}{X_{G1} - X_{G2}}\right)}{\pi.a_0}}.\sqrt{sec\left(\frac{\pi.a_0}{w}\right)} \times f_i + \sigma_{f,G1} \times$$

$$f_{G1} + \sigma_{f,G2} \times f_{G2} \quad (22)$$

For linear variation of E_i and exponential variation of γ_i in the graded region:

$$\sigma_{f,CP1}^{7} = \sum_{i=1}^{m} \sqrt{\frac{2\left(\frac{E_{G1}(X_i - X_{G2}) - E_{G2}(X_i - X_{G1})}{X_{G1} - X_{G2}}\right).\gamma_{G1}.\left(\frac{\gamma_{G1}}{\gamma_{G2}}\right)^{\left(\frac{X_i - X_{G1}}{X_{G1} - X_{G2}}\right)}}{\pi.a_0}}.\sqrt{sec\left(\frac{\pi.a_0}{w}\right)} \times f_i + \sigma_{f,G1} \times f_{G1} +$$

$$\sigma_{f,G2} \times f_{G2} \quad (23)$$

For linear variation of E_i and power-law variation of γ_i in the graded region:

$$\sigma_{f,CP1}^{8}=\sum_{i=1}^{m}\sqrt{\frac{2\left(\frac{E_{G1}(X_i-X_{G2})-E_{G2}(X_i-X_{G1})}{X_{G1}-X_{G2}}\right).\gamma_{G1}.\left(\frac{X_i}{X_{G1}}\right)^{\left[ln\left(\frac{\gamma_{G2}}{\gamma_{G1}}\right)/ln\left(\frac{X_{G2}}{X_{G1}}\right)\right]}}{\pi.a_0}}.\sqrt{sec\left(\frac{\pi.a_0}{w}\right)}\times f_i+\sigma_{f,G1}\times f_{G1}+\sigma_{f,G2}\times f_{G2} \quad (24)$$

And finally, for linear variation of both E_i and γ_i in the graded region:

$$\sigma_{f,CP1}^{9}=\sum_{i=1}^{m}\sqrt{\frac{2\left((E_{G1}+\gamma_{G1})(X_i-X_{G2})-(E_{G2}+\gamma_{G2})(X_i-X_{G1})\right)}{\pi.a_0(X_{G1}-X_{G2})}}.\sqrt{sec\left(\frac{\pi.a_0}{w}\right)}\times f_i+\sigma_{f,G1}\times f_{G1}+\sigma_{f,G2}\times f_{G2} \quad (25)$$

The results obtained from the whole nine proposed equations together with that obtained by experiment have been given in Table 3. Additionally, the deviations of the predicted results from the experimental one have been illustrated in the table. It is evident that utilizing exponential function for representing the variations of modulus of elasticity and power-low function for representing the variations of surface energy in the functionally graded region has resulted in the best performance model. On the whole, the performance of the models is better for CP1 crack configuration by using exponential function for representing the variations for both modulus of elasticity and surface energy as illustrated in Table 3. Therefore, one may suggest the models presented here for prediction the fracture strength of FGG structures with CP1 crack configuration.

3.1. Modelling of fracture strength of CP2 crack configuration

Fracture strength of the proposed FGG structure with crack configuration of CP2 can be considered as a combination of three parts according to Eq. (26):

$$\sigma_{f,CP2}=P\sigma_{f,CP2}^{FGG}+Q\sigma_{f,CP2}^{G1}+R\sigma_{f,CP2}^{G2} \quad (26)$$

where $\sigma_{f,CP2}^{FGG}$, $\sigma_{f,CP2}^{G1}$ and $\sigma_{f,CP2}^{G2}$ are fracture strength of FGG, G1 and G2 regions respectively

and *P*, *Q* and *R* are constants.

Modelling of fracture strength in this crack configuration is more complicated rather than CP1 crack configuration and is not simply carried out by considering a_0 as the crack length for the whole region. For G1 region, the whole chemical composition is constant and the fracture strength of a specimen with crack length of a_0 is calculated by Eq. (1). However, the whole material is not homogeneous and this thickness can only share into some parts of the final fracture strength. After that crack propagates in G1 region and spread into graded region, its length is no longer a_0. Therefore, the effective crack length, $a_{eff,i}$, is defined here as:

$$a_{i,eff} = a_0 + t_{G1} + \sum_{i=1}^{m}(i-1).t \tag{27}$$

where *t* is the thickness of each layer in functionally graded region and t_{G1} is the thickness of G1 region.

Consequently, when the crack reaches the first layer of the graded region, by considering that the whole specimen along the crack path is made from this layer, the fracture strength of the specimen with this new crack length is defined as:

$$\sigma_{f,CP2}^{FGG,i} = \sqrt{\frac{2E_i.\gamma_i}{\pi.\left(a_0+t_{G1}+\sum_{i=1}^{m}(i-1).t\right)}}.\sqrt{sec\left(\frac{\pi.\left(a_0+t_{G1}+\sum_{i=1}^{m}(i-1).t\right)}{w}\right)} \tag{28}$$

where $\sigma_{f,CP2}^{FGG,i}$ is the fracture strength of each layer with its corresponding effective crack length.

Same procedure could be followed by the constituent layers of functionally graded region. After transition of crack in functionally graded region, it will reach to G2 structure and the fracture strength of the remained material in FGG specimen can be calculated as following:

$$\sigma_{f,CP2}^{G2} = \sqrt{\frac{2E_{G2}.\gamma_{G2}}{\pi.(a_0+t_{G1}+t_{FGG})}}.\sqrt{sec\left(\frac{\pi.(a_0+t_{G1}+t_{FGG})}{w}\right)} \quad (29)$$

It is not possible to simply represent the fracture strength of the FGG specimen with CP2 crack configuration as an addition of $\sigma_{f,CP2}^{FGG}$, $\sigma_{f,CP2}^{G1}$ and $\sigma_{f,CP2}^{G2}$. In fact, the crack length has an important role in determining the share of each region on fracture strength of the considered FGG structure. Unfortunately, no exact formulation has been reported in the literature for this condition. Therefore, a new approach is presented here based of the functionally graded changes of fracture strength with respect to the crack length. According to Fig. 5, the specimen may be considered as a structure with crack length of a_0 and the required crack propagation path of *t*, equal to the thickness of the un-notched part of the specimen. The crack length directly affects on the fracture strength of the structure and it can be easily found from Eq. (1) that in a finite specimen with only 10 % increase in the initial crack length, the fracture strength is drastically decreased. Therefore, it is believed that the share of G1 region of the FGG structure with crack length of a_0 is more than that of functionally graded region with crack length of $[a_0 + t_{G1} + \sum_{i=1}^{m}(i-1).t]$. Therefore, an exponential function is defined here for representing the variations of the fracture strength share of each region, $f_{E,i}$, with respect to the thickness of the un-notched part of the specimen:

$$f_{E,i} = C.exp(t_i) + D \quad (30)$$

where t_i is the thickness of each region and *C* and *D* are constants which could be determined by the following boundary conditions:

If $t_i = t$ then $f_{E,i} = 1$, and

If $t_i = 0$ then $f_{E,i} = 0$,

By substituting the boundary conditions into Eq. (30), the following equation is

derived for representing the share of each layer on fracture strength of the considered FGG structure:

$$f_{E,i} = \frac{(1-exp(t_i))}{1-exp(t)} \quad (31)$$

By considering Fig. 5, it is estimated that the share of G1 region on final fracture strength, $f_{E,i}(G1)$, of the specimen is related to the area under the function between t_{G1} and t divided by the area under the whole function. In other words:

$$f_{E,i}(G1) = \frac{\int_0^{t_{G1}}(1-exp(t))dt}{\int_0^{t}(1-exp(t))dt} \quad (32)$$

Same procedure could be carried out for calculating each the share of each layer of functionally graded region on final fracture strength, $f_{E,i}(FGG,i)$:

$$f_{E,i}(FGG,i) = \frac{\int_{t_{G1}}^{t_{G1}+\sum_{i=1}^{m}(i-1).t}(1-exp(t))dt}{\int_0^{t}(1-exp(t))dt} \quad (33)$$

For G2 region, no share calculation is required because when the crack reaches this region, the specimen is considered as one with the crack length of $a_0 + t_{G1} + t_{FGG}$.

Therefore, Eq. (26) could be modified as following:

$$\sigma_{f,CP2} = \sum_{i=1}^{m} f_{E,i}(FGG,i)\sigma_{f,CP2}^{FGG} + f_{E,i}(G1)\sigma_{f,CP2}^{G1} + \sigma_{f,CP2}^{G2} \quad (34)$$

Finally, by substituting Eqs. (1)-(7), (28), (29), (32) and (33) into Eq. (34), the following nine proposed final equations could be represented for prediction fracture strength of the considered FGG structure with CP2 crack configuration:

For exponential variation of both E_i and γ_i in the graded region:

$\sigma_{f,CP2}^{1} =$

$$\sum_{i=1}^{m}\sqrt{\frac{2E_{G1}.\gamma_{G1}.\left(\frac{E_{G1}.\gamma_{G1}}{E_{G2}.\gamma_{G2}}\right)^{\left(\frac{X_i-X_{G1}}{X_{G1}-X_{G2}}\right)}}{\pi.\left(a_0+t_{G1}+\sum_{i=1}^{m}(i-1).t\right)}}.\sqrt{sec\left(\frac{\pi.\left(a_0+t_{G1}+\sum_{i=1}^{m}(i-1).t\right)}{w}\right)}.\frac{\int_{t_{G1}}^{t_{G1}+\sum_{i=1}^{m}(i-1).t}(1-exp(t))dt}{\int_0^t(1-exp(t))dt}+$$

$$\sqrt{\frac{2E_{G1}.\gamma_{G1}}{\pi.a_0}}.\sqrt{sec\left(\frac{\pi.a_0}{w}\right)}.\frac{\int_0^{t_{G1}}(1-exp(t))dt}{\int_0^t(1-exp(t))dt}+\sqrt{\frac{2E_{G2}.\gamma_{G2}}{\pi.(a_0+t_{G1}+t_{FGG})}}.\sqrt{sec\left(\frac{\pi.(a_0+t_{G1}+t_{FGG})}{w}\right)} \quad (35)$$

For exponential variation of E_i and power-law variation of γ_i in the graded region:

$$\sigma_{f,CP2}^{2}=$$

$$\sum_{i=1}^{m}\sqrt{\frac{2E_{G1}.\gamma_{G1}.\left(\frac{E_{G1}}{E_{G2}}\right)^{\left(\frac{X_i-X_{G1}}{X_{G1}-X_{G2}}\right)}.\left(\frac{X_i}{X_{G1}}\right)^{\left[ln\left(\frac{\gamma_{G2}}{\gamma_{G1}}\right)/ln\left(\frac{X_{G2}}{X_{G1}}\right)\right]}}{\pi.\left(a_0+t_{G1}+\sum_{i=1}^{m}(i-1).t\right)}}.\sqrt{sec\left(\frac{\pi.\left(a_0+t_{G1}+\sum_{i=1}^{m}(i-1).t\right)}{w}\right)}.\frac{\int_{t_{G1}}^{t_{G1}+\sum_{i=1}^{m}(i-1).t}(1-exp(t))dt}{\int_0^t(1-exp(t))dt}+$$

$$\sqrt{\frac{2E_{G1}.\gamma_{G1}}{\pi.a_0}}.\sqrt{sec\left(\frac{\pi.a_0}{w}\right)}.\frac{\int_0^{t_{G1}}(1-exp(t))dt}{\int_0^t(1-exp(t))dt}+\sqrt{\frac{2E_{G2}.\gamma_{G2}}{\pi.(a_0+t_{G1}+t_{FGG})}}.\sqrt{sec\left(\frac{\pi.(a_0+t_{G1}+t_{FGG})}{w}\right)} \quad (36)$$

For exponential variation of E_i and linear variation of γ_i in the graded region:

$$\sigma_{f,CP2}^{3}=$$

$$\sum_{i=1}^{m}\sqrt{\frac{2E_{G1}.\left(\frac{E_{G1}}{E_{G2}}\right)^{\left(\frac{X_i-X_{G1}}{X_{G1}-X_{G2}}\right)}.\left(\frac{\gamma_{G1}(X_i-X_{G2})-\gamma_{G2}(X_i-X_{G1})}{X_{G1}-X_{G2}}\right)}{\pi.\left(a_0+t_{G1}+\sum_{i=1}^{m}(i-1).t\right)}}.\sqrt{sec\left(\frac{\pi.\left(a_0+t_{G1}+\sum_{i=1}^{m}(i-1).t\right)}{w}\right)}.\frac{\int_{t_{G1}}^{t_{G1}+\sum_{i=1}^{m}(i-1).t}(1-exp(t))dt}{\int_0^t(1-exp(t))dt}+$$

$$\sqrt{\frac{2E_{G1}.\gamma_{G1}}{\pi.a_0}}.\sqrt{sec\left(\frac{\pi.a_0}{w}\right)}.\frac{\int_0^{t_{G1}}(1-exp(t))dt}{\int_0^t(1-exp(t))dt}+\sqrt{\frac{2E_{G2}.\gamma_{G2}}{\pi.(a_0+t_{G1}+t_{FGG})}}.\sqrt{sec\left(\frac{\pi.(a_0+t_{G1}+t_{FGG})}{w}\right)} \quad (37)$$

For power-law variation of E_i and exponential variation of γ_i in the graded region:

$$\sigma_{f,CP2}^{4}=$$

$$\sum_{i=1}^{m}\sqrt{\frac{2E_{G1}.\gamma_{G1}.\left(\frac{X_i}{X_{G1}}\right)^{\left[ln\left(\frac{E_{G2}}{E_{G1}}\right)/ln\left(\frac{X_{G2}}{X_{G1}}\right)\right]}.\left(\frac{\gamma_{G1}}{\gamma_{G2}}\right)^{\left(\frac{X_i-X_{G1}}{X_{G1}-X_{G2}}\right)}}{\pi.\left(a_0+t_{G1}+\sum_{i=1}^{m}(i-1).t\right)}}.\sqrt{sec\left(\frac{\pi.\left(a_0+t_{G1}+\sum_{i=1}^{m}(i-1).t\right)}{w}\right)}.\frac{\int_{t_{G1}}^{t_{G1}+\sum_{i=1}^{m}(i-1).t}(1-exp(t))dt}{\int_0^t(1-exp(t))dt}+$$

$$\sqrt{\frac{2E_{G1}.\gamma_{G1}}{\pi.a_0}}.\sqrt{sec\left(\frac{\pi.a_0}{w}\right)}.\frac{\int_0^{t_{G1}}(1-exp(t))dt}{\int_0^t(1-exp(t))dt}+\sqrt{\frac{2E_{G2}.\gamma_{G2}}{\pi.(a_0+t_{G1}+t_{FGG})}}.\sqrt{sec\left(\frac{\pi.(a_0+t_{G1}+t_{FGG})}{w}\right)} \quad (38)$$

For power-law variation of both E_i and γ_i in the graded region:

$$\sigma_{f,CP2}^{5} =$$

$$\sum_{i=1}^{m}\sqrt{\frac{2E_{G1}.\gamma_{G1}.\left(\frac{X_i}{X_{G1}}\right)^{\left[ln\left(\frac{E_{G2}}{E_{G1}}\right).ln\left(\frac{\gamma_{G2}}{\gamma_{G1}}\right)/\left[ln\left(\frac{X_{G2}}{X_{G1}}\right)\right]^2\right]}}{\pi.\left(a_0+t_{G1}+\sum_{i=1}^{m}(i-1).t\right)}}.\sqrt{sec\left(\frac{\pi.\left(a_0+t_{G1}+\sum_{i=1}^{m}(i-1).t\right)}{w}\right)}.\frac{\int_{t_{G1}}^{t_{G1}+\sum_{i=1}^{m}(i-1).t}(1-exp(t))dt}{\int_0^t(1-exp(t))dt}+$$

$$\sqrt{\frac{2E_{G1}.\gamma_{G1}}{\pi.a_0}}.\sqrt{sec\left(\frac{\pi.a_0}{w}\right)}.\frac{\int_0^{t_{G1}}(1-exp(t))dt}{\int_0^t(1-exp(t))dt}+\sqrt{\frac{2E_{G2}.\gamma_{G2}}{\pi.(a_0+t_{G1}+t_{FGG})}}.\sqrt{sec\left(\frac{\pi.(a_0+t_{G1}+t_{FGG})}{w}\right)} \qquad (39)$$

For power-law variation of E_i and linear variation of γ_i in the graded region:

$$\sigma_{f,CP2}^{6} =$$

$$\sum_{i=1}^{m}\sqrt{\frac{2E_{G1}.\left(\frac{X_i}{X_{G1}}\right)^{\left[ln\left(\frac{E_{G2}}{E_{G1}}\right)/ln\left(\frac{X_{G2}}{X_{G1}}\right)\right]}.\left(\frac{\gamma_{G1}(X_i-X_{G2})-\gamma_{G2}(X_i-X_{G1})}{X_{G1}-X_{G2}}\right)}{\pi.\left(a_0+t_{G1}+\sum_{i=1}^{m}(i-1).t\right)}}.\sqrt{sec\left(\frac{\pi.\left(a_0+t_{G1}+\sum_{i=1}^{m}(i-1).t\right)}{w}\right)}.\frac{\int_{t_{G1}}^{t_{G1}+\sum_{i=1}^{m}(i-1).t}(1-exp(t))dt}{\int_0^t(1-exp(t))dt}+$$

$$\sqrt{\frac{2E_{G1}.\gamma_{G1}}{\pi.a_0}}.\sqrt{sec\left(\frac{\pi.a_0}{w}\right)}.\frac{\int_0^{t_{G1}}(1-exp(t))dt}{\int_0^t(1-exp(t))dt}+\sqrt{\frac{2E_{G2}.\gamma_{G2}}{\pi.(a_0+t_{G1}+t_{FGG})}}.\sqrt{sec\left(\frac{\pi.(a_0+t_{G1}+t_{FGG})}{w}\right)} \qquad (40)$$

For linear variation of E_i and exponential variation of γ_i in the graded region:

$$\sigma_{f,CP2}^{7} =$$

$$\sum_{i=1}^{m}\sqrt{\frac{2\left(\frac{E_{G1}(X_i-X_{G2})-E_{G2}(X_i-X_{G1})}{X_{G1}-X_{G2}}\right).\gamma_{G1}.\left(\frac{\gamma_{G1}}{\gamma_{G2}}\right)^{\left(\frac{X_i-X_{G1}}{X_{G1}-X_{G2}}\right)}}{\pi.\left(a_0+t_{G1}+\sum_{i=1}^{m}(i-1).t\right)}}.\sqrt{sec\left(\frac{\pi.\left(a_0+t_{G1}+\sum_{i=1}^{m}(i-1).t\right)}{w}\right)}.\frac{\int_{t_{G1}}^{t_{G1}+\sum_{i=1}^{m}(i-1).t}(1-exp(t))dt}{\int_0^t(1-exp(t))dt}+$$

$$\sqrt{\frac{2E_{G1}.\gamma_{G1}}{\pi.a_0}}.\sqrt{sec\left(\frac{\pi.a_0}{w}\right)}.\frac{\int_0^{t_{G1}}(1-exp(t))dt}{\int_0^t(1-exp(t))dt}+\sqrt{\frac{2E_{G2}.\gamma_{G2}}{\pi.(a_0+t_{G1}+t_{FGG})}}.\sqrt{sec\left(\frac{\pi.(a_0+t_{G1}+t_{FGG})}{w}\right)} \qquad (41)$$

For linear variation of E_i and power-law variation of γ_i in the graded region:

$$\sigma_{f,CP2}^{8} =$$

$$\sum_{i=1}^{m}\sqrt{\frac{2\left(\frac{E_{G1}(X_i-X_{G2})-E_{G2}(X_i-X_{G1})}{X_{G1}-X_{G2}}\right).\gamma_{G1}.\left(\frac{X_i}{X_{G1}}\right)^{\left[ln\left(\frac{\gamma_{G2}}{\gamma_{G1}}\right)/ln\left(\frac{X_{G2}}{X_{G1}}\right)\right]}}{\pi.\left(a_0+t_{G1}+\sum_{i=1}^{m}(i-1).t\right)}}.\sqrt{sec\left(\frac{\pi.\left(a_0+t_{G1}+\sum_{i=1}^{m}(i-1).t\right)}{w}\right)}.\frac{\int_{t_{G1}}^{t_{G1}+\sum_{i=1}^{m}(i-1).t}(1-exp(t))dt}{\int_0^t(1-exp(t))dt}+$$

$$\sqrt{\frac{2E_{G1}.\gamma_{G1}}{\pi.a_0}}.\sqrt{sec\left(\frac{\pi.a_0}{w}\right)}.\frac{\int_0^{t_{G1}}(1-exp(t))dt}{\int_0^{t}(1-exp(t))dt}+\sqrt{\frac{2E_{G2}.\gamma_{G2}}{\pi.(a_0+t_{G1}+t_{FGG})}}.\sqrt{sec\left(\frac{\pi.(a_0+t_{G1}+t_{FGG})}{w}\right)} \quad (42)$$

And finally, for linear variation of both E_i and γ_i in the graded region:

$$\sigma_{f,CP2}^{9} =$$

$$\sum_{i=1}^{m}\sqrt{\frac{2\left((E_{G1}+\gamma_{G1})(X_i-X_{G2})-(E_{G2}+\gamma_{G2})(X_i-X_{G1})\right)}{\pi.(a_0+t_{G1}+\sum_{i=1}^{m}(i-1).t).(X_{G1}-X_{G2})}}.\sqrt{sec\left(\frac{\pi.(a_0+t_{G1}+\sum_{i=1}^{m}(i-1).t)}{w}\right)}.\frac{\int_{t_{G1}}^{t_{G1}+\sum_{i=1}^{m}(i-1).t}(1-exp(t))dt}{\int_0^{t}(1-exp(t))dt}+$$

$$\sqrt{\frac{2E_{G1}.\gamma_{G1}}{\pi.a_0}}.\sqrt{sec\left(\frac{\pi.a_0}{w}\right)}.\frac{\int_0^{t_{G1}}(1-exp(t))dt}{\int_0^{t}(1-exp(t))dt}+\sqrt{\frac{2E_{G2}.\gamma_{G2}}{\pi.(a_0+t_{G1}+t_{FGG})}}.\sqrt{sec\left(\frac{\pi.(a_0+t_{G1}+t_{FGG})}{w}\right)} \quad (43)$$

The results obtained from the nine proposed equations together with that obtained by experiment have been given in Table 4. Furthermore, the deviations of the predicted results from the experimental one have been illustrated in the table. It is evident that utilizing linear function for representing the variations of modulus of elasticity and exponential function for representing the variations of surface energy in the functionally graded region has resulted in the best performance model. On the whole, similar to the results obtained for CP1 crack configuration the performance of the models is better for CP2 crack configuration by using exponential function for representing the variations for both modulus of elasticity and surface energy as illustrated in Table 4. Therefore, one may suggest the models presented here for prediction the fracture strength of FGG structures with CP1 crack configuration.

It should be noted that the models presented for CP2 crack configuration were considered for the case that crack is situated at G1 region of the specimen. Same equations for CP2 crack configuration and crack situated in G2 region could be derived by changing the indices G1 and G2 in Eqs. (35)-(43) together. An additional modelling was conducted by this crack situation and the results were listed in Table 5. Once more, utilizing linear function for representing the variations of modulus of elasticity and exponential function for representing the variations of surface energy in the functionally graded region has resulted in the best

performance model. This is why the exponential function for representing the gradual change of both modulus of elasticity and surface energy has been resulted in higher performance models again.

The interesting point is the difference between fracture strength of FGG structure with CP2 crack configuration and different crack tip situations in G1 or G2 regions. This shows the different share of fracture energy considered in the modelling procedure. While crack initiates its propagation from G1 region, it requires lower energy with respect to the situation that crack begins its growth from G2 region. This is confirmed by the difference between their surface energy which is 12.9 MJ for G1 specimen and 24.5 MJ for G2 specimen. According to the proposed model, the main share of fracture energy is related to the regions that are ahead the crack tip. Therefore, this confirms again the accuracy of the model and energy share considered for CP2 crack configuration.

4. Conclusions

In the present study, fracture strength of FGG structure with CP1 and CP2 crack configurations was analytically modelled. FGG structures were produced by pouring a 2-layer specimen and subsequent vibration after each level of pouring where the mixture proportion and chemical composition of the two layers were different. Functionally graded region with the depth of 18.6 mm was created due to the diffusion of different mixtures into each other. To conduct the modelling, the functionally graded region was considered as a section with 372 layers where the thickness of each layer was considered 50 μm. For each CP1 and CP2 modelling method, nine equations were derived. The difference between the equations was in their utilized function for representing modulus of elasticity and surface energy in the graded region of FGG structure. However, the best model for CP1 crack configuration was achieved by utilizing exponential function for the variations of modulus of

elasticity and power-law function for the variations of surface energy. The experimental flexural strength for CP1 crack configuration was 6.5 MPa while the best performance model resulted in flexural strength of 6.4 MPa with +3.23 % of deviation from experimental results. Furthermore, the best model for CP2 crack configuration was achieved by utilizing linear function for the variations of modulus of elasticity and exponential function for the variations of surface energy. The experimental flexural strength for CP2 crack configuration with crack in G1 and G2 regions were 5.8 and 6.9 MPa respectively where the best performance models revealed the values of 5.9 and 7.0 MPa respectively with the deviations of +1.72 and +1.45 % respectively.

References

[1] Wen, X. D., Tu, J. L., & Gan, W. Z. (2013). Durability protection of the functionally graded structure concrete in the splash zone. *Constr Build Mat*, *41*, 246-251.

[2] Nazari, A., Mohandesi, J. A., & Riahi, S. (2011). Modeling fracture toughness of functionally graded steels in crack arrester configuration. *Comp Mat Sci*, *50*(4), 1578-1586.

[3] Carreño, F., Chao, J., Pozuelo, M., & Ruano, O. A. (2003). Microstructure and fracture properties of an ultrahigh carbon steel–mild steel laminated composite. *Scripta Materialia*, *48*(8), 1135-1140.

[4] Dias, C. M. R., Savastano Jr, H., & John, V. M. (2010). Exploring the potential of functionally graded materials concept for the development of fiber cement. *Constr Build Mat*, *24*(2), 140-146.

[5] Shen, B., Hubler, M., Paulino, G. H., & Struble, L. J. (2008). Functionally-graded fiber-reinforced cement composite: Processing, microstructure, and properties. *Cem Concr*

Compos, *30*(8), 663-673.

[6] Quek, S. T., Lin, V. W. J., & Maalej, M. (2010). Development of functionally-graded cementitious panel against high-velocity small projectile impact. *Int J Impact Eng*, *37*(8), 928-941.

[7] Ryu, G. S., Lee, Y. B., Koh, K. T., & Chung, Y. S. (2013). The mechanical properties of fly ash-based geopolymer concrete with alkaline activators. *Constr Build Mat 47*, 409-418.

[8] Hanjitsuwan, S., Hanpratub, S., Thongbai, P., Maensiri, S., Sata, V., & Chindaprasirt, P. (2014). Effects of NaOH concentrations on physical and electrical properties of high calcium fly ash geopolymer paste. *Cem Concr Compos*, *45*, 9-14.

[9] Li, Q., Xu, H., Li, F., Li, P., Shen, L., & Zhai, J. (2012). Synthesis of geopolymer composites from blends of CFBC fly and bottom ashes. *Fuel*, *97*, 366-372.

[10] Alex, T.C., Kalinkin, A.M., Nath, S.K., Gurevich, B.I.,Kalinkina, E.V., Tyukavkina, V.V., & Kumar, S. (2013). Utilization of zinc slag through geopolymerization: Influence of milling atmosphere. *Int J Mineral Process*, *123*, 102-107.

[11] Komnitsas, K., Zaharaki, D., & Perdikatsis, V. (2009). Effect of synthesis parameters on the compressive strength of low-calcium ferronickel slag inorganic polymers. *J Hazard Mater*, *161 (2-3)*, 760-768.

[12] Kalinkin, A.M., Kumar, S., Gurevich, B.I., Alex, T.C., Kalinkina, E.V., Tyukavkina, V.V.,Kalinnikov, V.T., and Kumar, R. (2012). Geopolymerization behavior of Cu-Ni slag mechanically activated in air and in CO 2 atmosphere. *Int J Mineral Process, 112-113,*101-106.

[13] Autef, A., Joussein, E., Poulesquen, A., Gasgnier, G., Pronier, S., Sobrados, I., Sanz, J., & Rossignol, S. (2013). Influence of metakaolin purities on potassium geopolymer formulation: the existence of several networks. *J colloid Interface sci, 408,* 43-58.

[14] ASTM C115, (2010) Standard Test Method for Fineness of Portland Cement by the Turbidimeter, United States of America: ASTM international.

[15] Hanjitsuwan, S., Hunpratub, S., Thongbai, P., Maensiri, S., Sata, V., & Chindaprasirt, P. (2014). Effects of NaOH concentrations on physical and electrical properties of high calcium fly ash geopolymer paste. Cem Concr Compos, 45, 9-14.

[16] Mijarsh, M. J. A., Johari, M., & Ahmad, Z. A. (2014). Synthesis of geopolymer from large amounts of treated palm oil fuel ash: Application of the Taguchi method in investigating the main parameters affecting compressive strength. *Constr Build Mat, 52*, 473-481.

[17] ASTM C469-87, (2001), ASTM Standards C469-87, 1987. Test Method for Static Modulus of Elasticity and Poisson's Ratio of Concrete in Compression, United States of America: ASTM international.

[18] Mozgawa, W., & Deja, J. (2009). Spectroscopic studies of alkaline activated slag geopolymers. *J Molecul Struct*, 924, 434-441.

[19] Zaharaki, D., Komnitsas, K., & Perdikatsis, V. (2010). Use of analytical techniques for identification of inorganic polymer gel composition. *J Mater Sci*, 45(10), 2715-2724.

[20] Lian, C., Zhuge, Y., & Beecham, S. (2011). The relationship between porosity and strength for porous concrete. *Constr Build Mat*, *25*(11), 4294-4298.

[21] Mohandesi, J. A., Namin, R. P., & Shahosseinie, M. H. (2006). Tensile behavior of functionally graded steels produced by electroslag remelting. *Met Mat Trans A*, *37*(7), 2125-2132.

[22] Latifi, M., Farhatnia, F., & Kadkhodaei, M. (2013). Buckling analysis of rectangular

functionally graded plates under various edge conditions using Fourier Series Expansion. *European J Mech-A/Solids*.

[23] Zhang, H., Zhao, X., & Su, J. (2012). Random dynamic response and reliability of a crack in a functionally graded material layer between two dissimilar elastic half-planes. *Eng Analysis Boundary Elements*, *36*(11), 1560-1570.

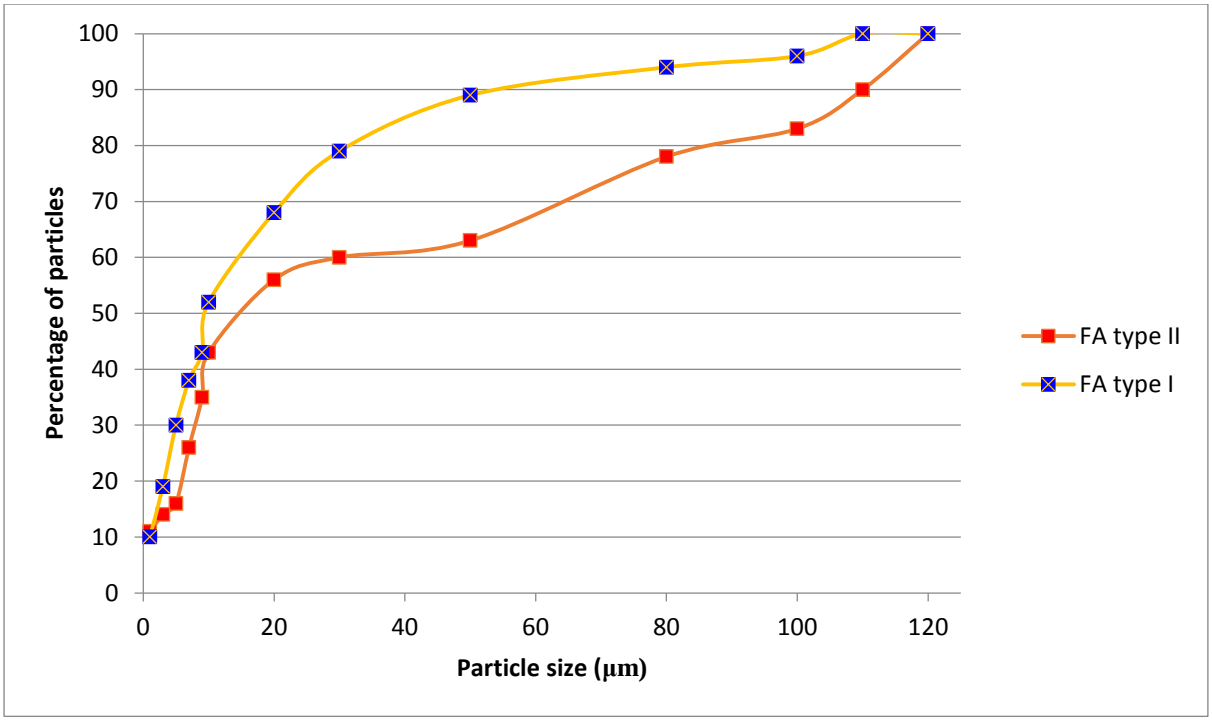

Fig. 1. Particle size distribution of fly ashes type I and II

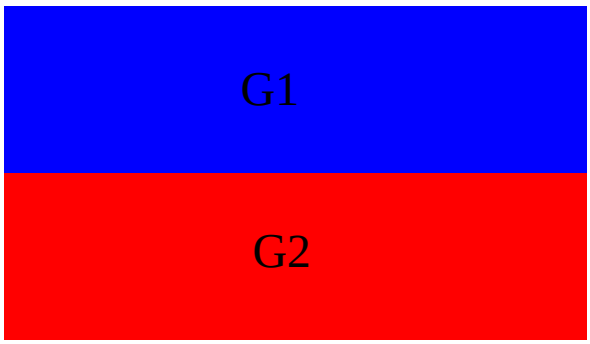

(a)

(b)

Fig. 2. Schematic illustration of the process for producing FGG structure, a) supposed two different layers of geopolymers, b) formation of functionally graded region during vibration and subsequent hardening

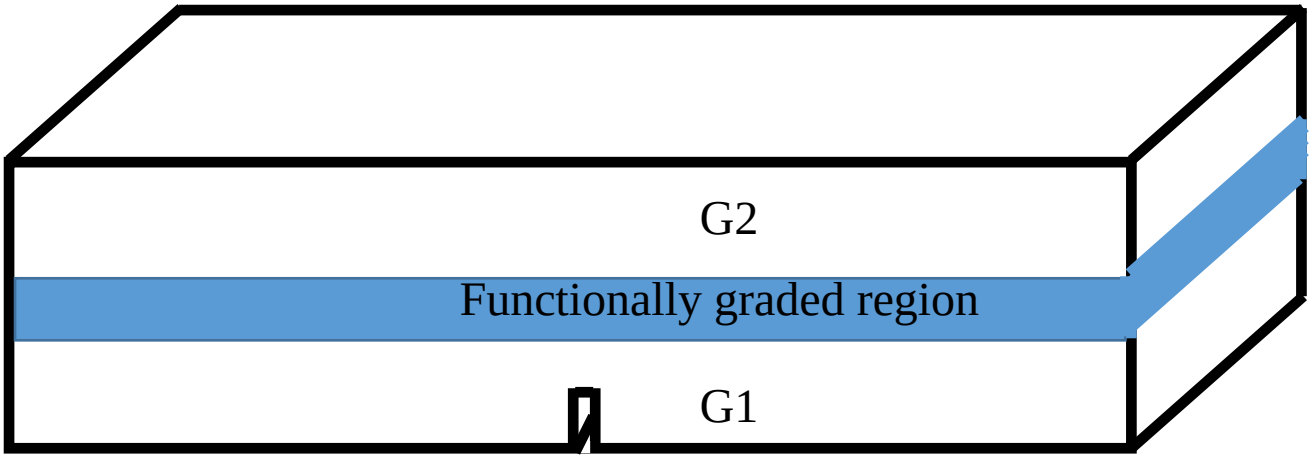

(a)

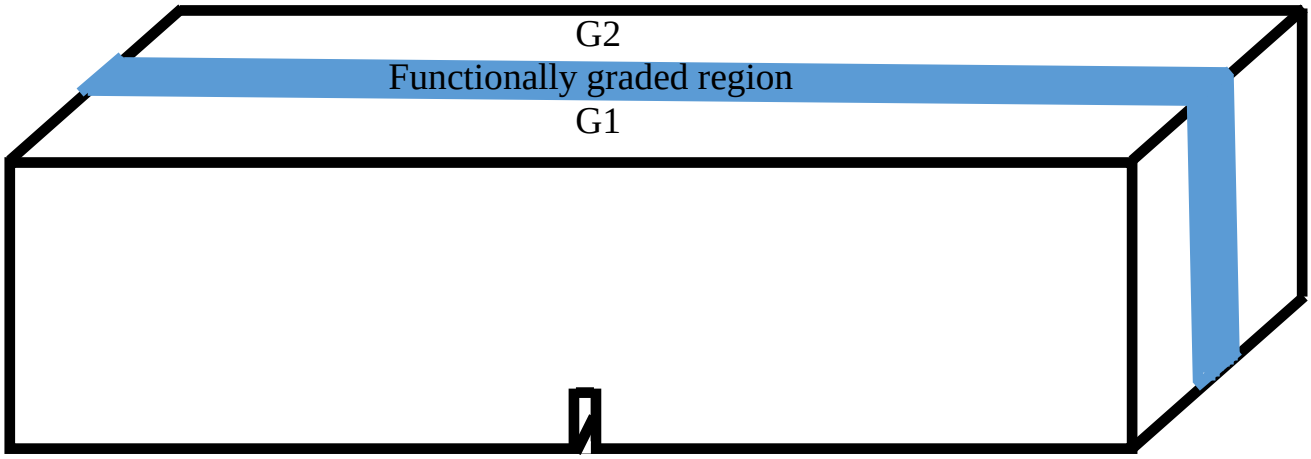

(b)

Fig. 3. Schematic illustration of crack configuration in FGG structure, a) CP2 and b) CP1 crack configurations

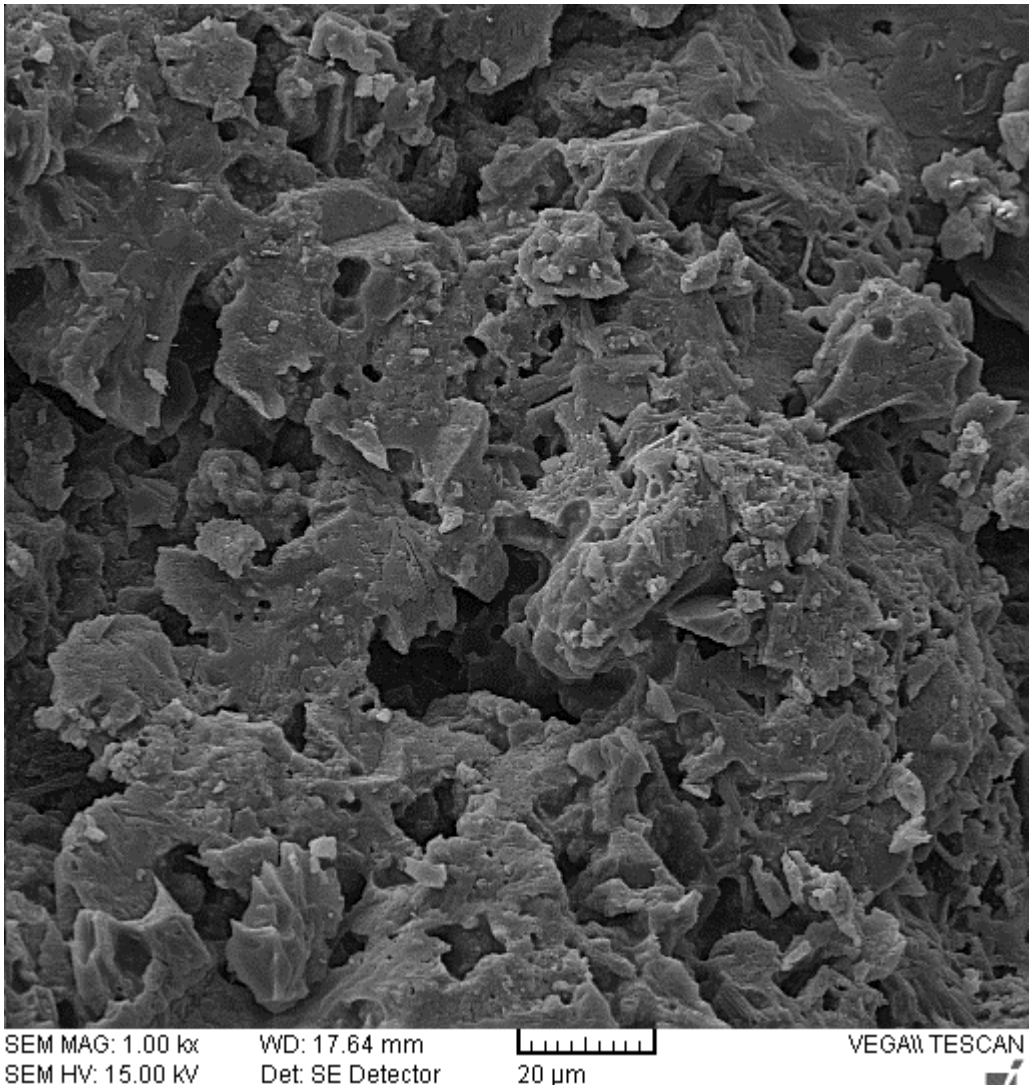
SEM MAG: 1.00 kx
SEM HV: 15.00 kV
WD: 17.64 mm
Det: SE Detector
20 µm
VEGA\\ TESCAN

(a)

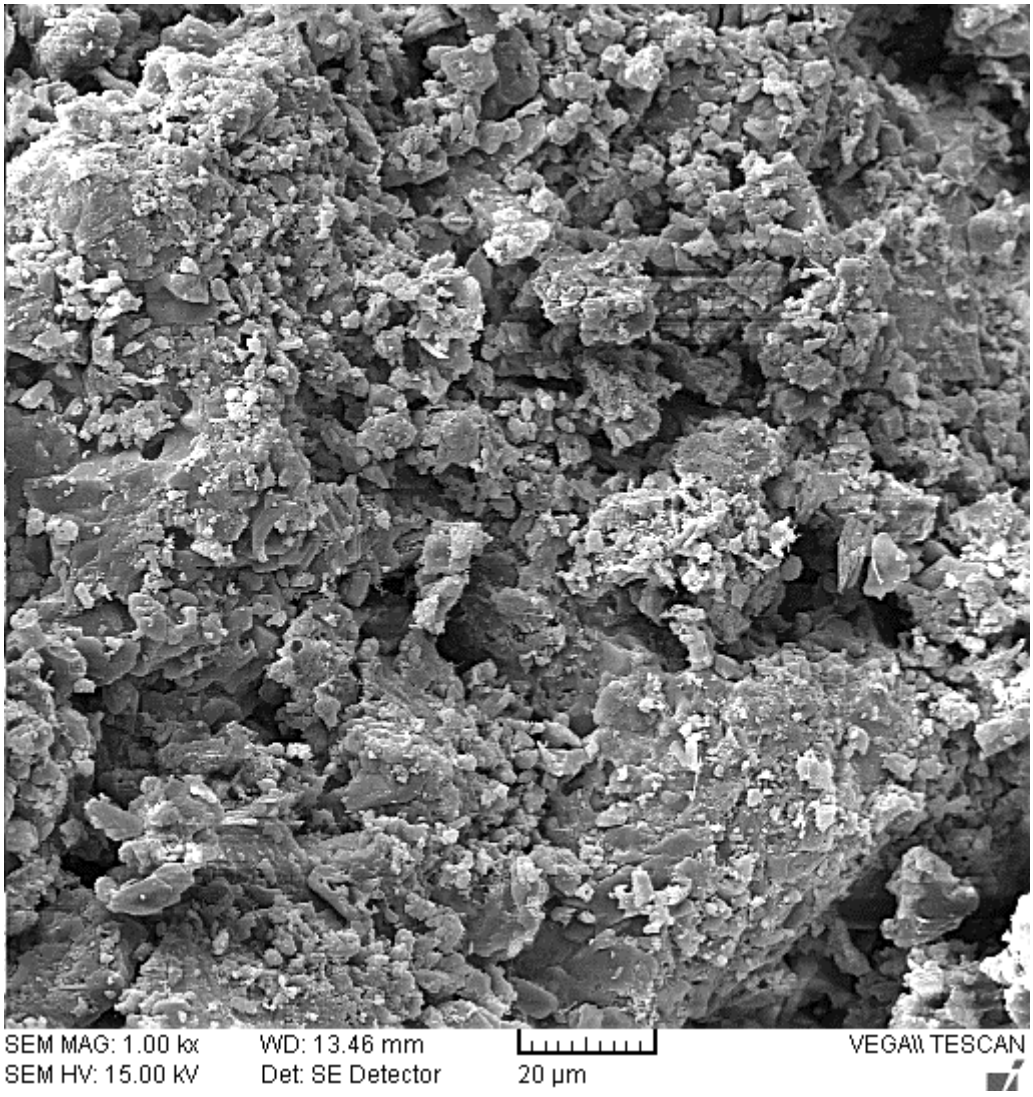
SEM MAG: 1.00 kx
SEM HV: 15.00 kV
WD: 13.46 mm
Det: SE Detector
20 µm
VEGA\\ TESCAN

(b)

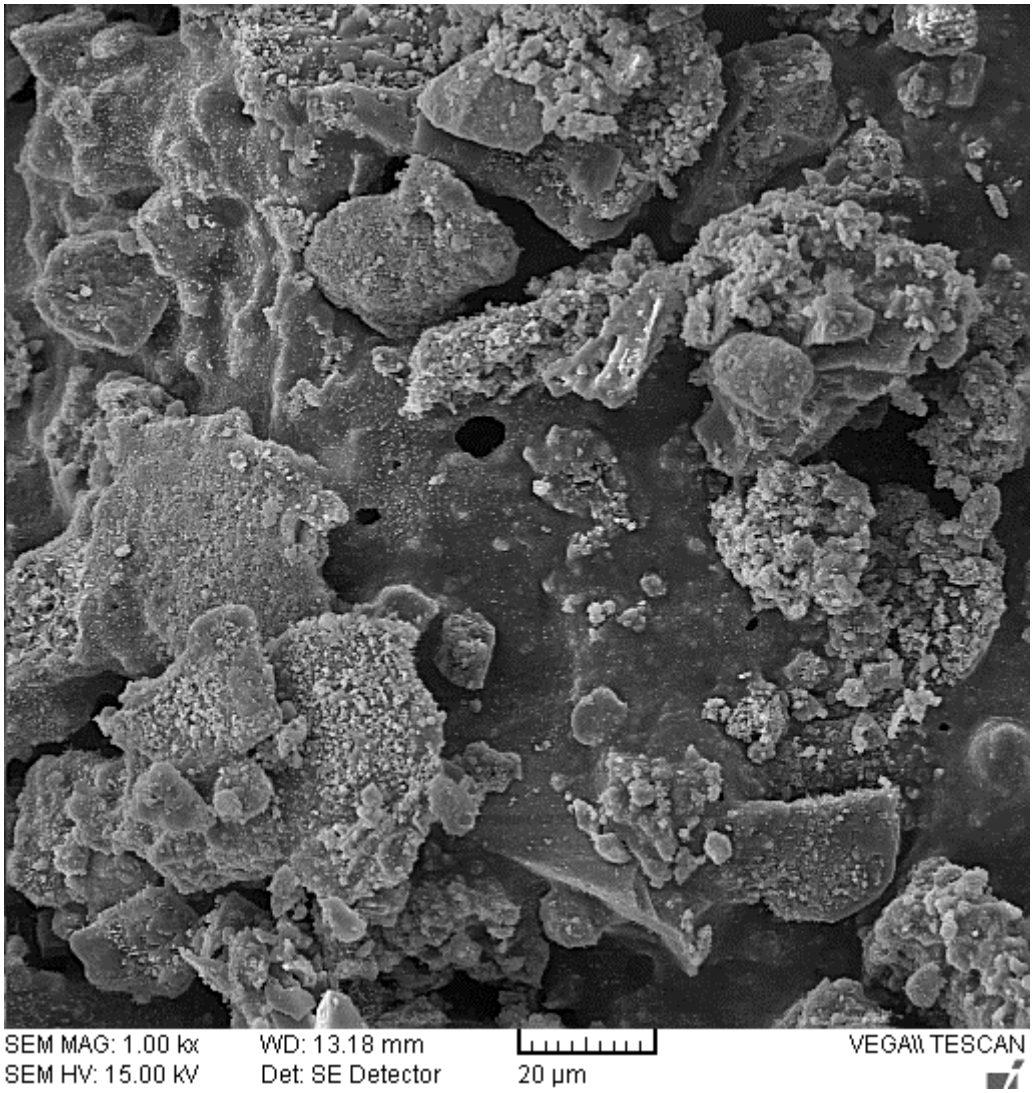

(c)

Fig. 4. SEM images of a) G1, b) G2 and c) FGG specimen

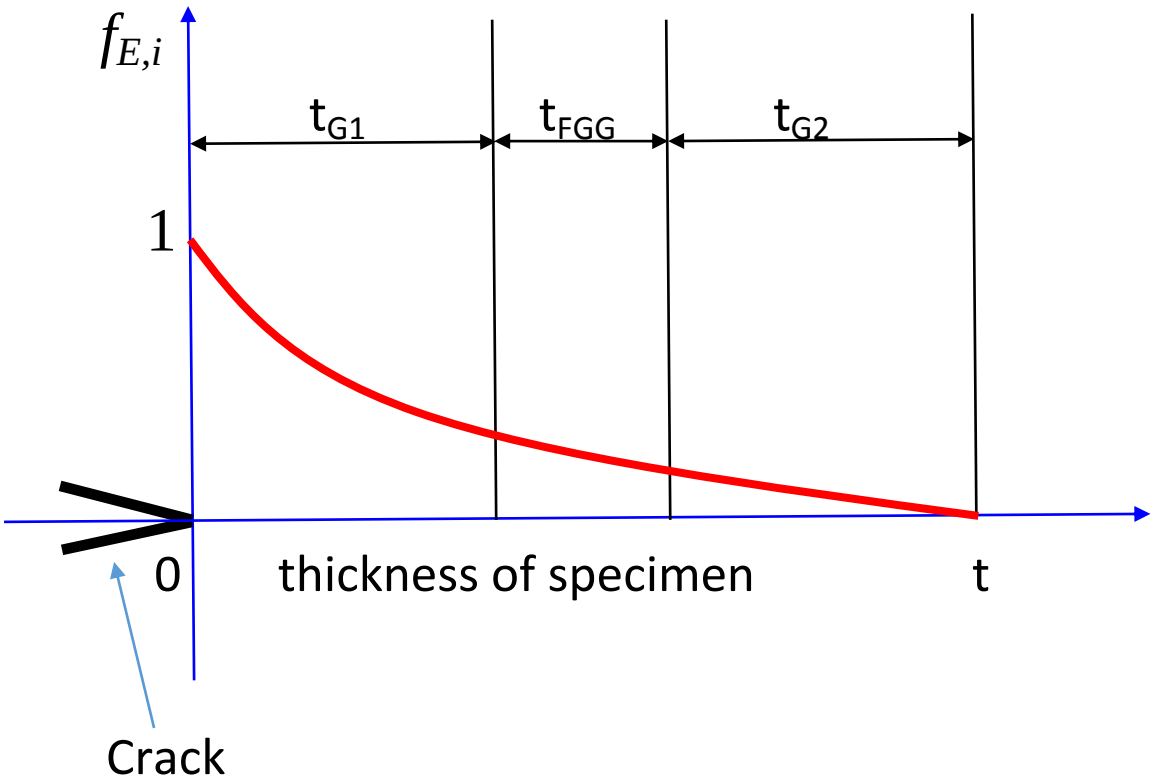

Fig. 5. Share of fracture energy of each region in the FGG specimen.

Table 1. Chemical composition of the utilized fly ashes and sodium silicate

Material	SiO_2	Al_2O_3	Fe_2O_3	CaO	SO_3	Na_2O	L.O.I.
FA type I	35.2	23.2	12.3	20.1	2.3	0.3	3.4
FA type II	62.7	22.1	2.5	3.1	0.5	0.4	2.6
Sodium silicate	37.8	-	-	-	-	12.3	-

Table 2. Fracture strength, modulus of elasticity and surface energy of G1 and G2 specimens

Material	G1	G2
Modulus of elasticity (GPa)	33	42
Fracture strength (MPa)	5.2	8.1
Surface energy (MJ)	12.9	24.5

Table 3. Comparison between experimental and predicted fracture strength of the FGG specimens with CP1 crack configuration

	Fracture strength (MPa)	Deviation from experimental
Experimental	6.2	0
$\sigma_{f,CP1}^{1}$	6.5	+ 4.84
$\sigma_{f,CP1}^{2}$	6.4	+ 3.23
$\sigma_{f,CP1}^{3}$	6.5	+ 4.84
$\sigma_{f,CP1}^{4}$	6.6	+ 6.45
$\sigma_{f,CP1}^{5}$	6.7	+ 8.06
$\sigma_{f,CP1}^{6}$	7.0	+ 12.9
$\sigma_{f,CP1}^{7}$	6.6	+ 6.45
$\sigma_{f,CP1}^{8}$	6.8	+ 9.68
$\sigma_{f,CP1}^{9}$	7.1	+ 14.5

Table 4. Comparison between experimental and predicted fracture strength of the FGG specimens with CP2 crack configuration with crack in G1 region

	Fracture strength (MPa)	Deviation from experimental
Experimental	5.8	0
$\sigma_{f,CP2}^{1}$	6.2	+ 6.90
$\sigma_{f,CP2}^{2}$	6.3	+ 8.62
$\sigma_{f,CP2}^{3}$	6.2	+ 6.90
$\sigma_{f,CP2}^{4}$	6.5	+ 12.1
$\sigma_{f,CP2}^{5}$	6.8	+ 17.2
$\sigma_{f,CP2}^{6}$	6.7	+ 15.5
$\sigma_{f,CP2}^{7}$	5.9	+ 1.72
$\sigma_{f,CP2}^{8}$	7.0	+ 20.7
$\sigma_{f,CP2}^{9}$	6.9	+ 19.0

Table 5. Comparison between experimental and predicted fracture strength of the FGG specimens with CP2 crack configuration with crack in G2 region

	Fracture strength (MPa)	Deviation from experimental
Experimental	6.9	0
$\sigma_{f,CP2}^{1}$	7.2	+ 4.35
$\sigma_{f,CP2}^{2}$	7.3	+ 5.80
$\sigma_{f,CP2}^{3}$	7.3	+ 5.80
$\sigma_{f,CP2}^{4}$	7.2	+ 4.35
$\sigma_{f,CP2}^{5}$	7.5	+ 8.70
$\sigma_{f,CP2}^{6}$	7.4	+ 7.25
$\sigma_{f,CP2}^{7}$	7.0	+ 1.45
$\sigma_{f,CP2}^{8}$	7.4	+ 7.25
$\sigma_{f,CP2}^{9}$	7.6	+ 10.2